Sustainable Energy Technologies and Assessments 48 (2021) 101624

Contents lists available at ScienceDirect

Sustainable Energy Technologies and Assessments

journal homepage: www.elsevier.com/locate/seta

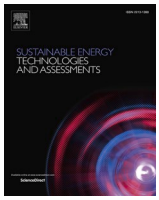

Extension of PC-SAFT equation of state to include mineral surface effect in fluid properties using molecular dynamic simulation

Sajjad Ahmadi Goltapeh [a,*], Saeed Abdolahi [b], Rohaldin Miri [c], Helge Hellevang [a]

[a] Department of Geosciences, University of Oslo, P.O. Box 1047 Blindern, 0316 Oslo, Norway
[b] Department of Chemical Engineering, Amirkabir University of Technology, 424 Hafez Avenue, Tehran, Iran
[c] School of Chemical Engineering, Iran University of Science and Technology (IUST), P.O. Box 16765-163, Tehran, Iran

ARTICLE INFO

Keywords:
Molecular Dynamic
PC-SAFT
Calcite-Water Interface
Thermodynamic Properties
Fluid-Mineral Interfacial Properties

ABSTRACT

In the vicinity of fluid-mineral interfaces a transition zone exist in which the order and packing of the molecules differ from that of the bulk phase where the distribution of intermolecular forces exhibit a more homogenous form. To develop an understanding of the thermodynamic properties in the fluid-mineral interface molecular dynamic (MD) simulation was conducted for the water-calcite system. To predict the water properties near the calcite wall, we have defined a contribution for Helmholtz energy extended from PC-SAFT equation of state (EOS). The new energy contribution depends on the confinement parameters i.e. potential of fluid-wall interaction, confinement degree, bulk density, and fraction of confined molecules estimated by MD simulation. The outcomes of MD simulation exhibit the layering transition of water on the water-calcite interface. In addition, MD simulation confirm the energy deviation within the layering transition zone, where the calcite adsorbs the water molecules. In this approach, the modified PC-SAFT showed a good agreement with MD observations. The results of this study can contribute to a better understanding of fluid behavior at the fluid-mineral interface. In addition, this technique is a valuable tool that can be used to estimate solubility limits in multicomponent fluid processing and pipeline transport.

Introduction

Energy has a significant role in social and economic developments. As the population grows, the demand for energy consumption increases. To mitigate the environmental impacts of the greenhouse gases, development of renewable energy resources is the prevalent solution. However, achieving the sustainable solutions with low impact on environment is a long-term plan. On the other hand, current renewable supplies are not enough to keep up with the energy demand and the need to traditional energy resources would remain. In order to achieve low carbon intensive systems, optimized methods in thermodynamic assessment of hydrocarbons play a significant role. Improved recovery from oil and gas reservoirs and cost-effective design of downstream facilities requires accurate knowledge of phase behavior and thermodynamic properties [1,2]. Equation of states (EOS) are suitable tools performing the thermodynamic properties calculation and phase behavior analysis. The EOSs define a mathematical relationship between the pressure (P), volume (V) and temperature (T). Then, all thermodynamic properties are computable with known relation between P, V and T. Most of the EOSs can be classified in three main categories i.e. virial, cubic and molecular-based. The virial EOS of high order are precise enough to cover a wide range of fluid types but they are not efficient because they need a large empirical database for convergence [3]. The most widely used EOSs in engineering applications are cubic EOSs which originally introduced by Van der Waals [4]. The conventional cubic EOSs although predict the behavior of simple components precisely but they suffer from lack of accuracy in describing the complex molecules and mixtures having strong intermolecular forces.

The molecular based EOSs so-called SAFT-type EOSs are constructed based on the statistical associating fluid theory and they formulate dispersive and associative interactions upon Barker-Henderson and Wertheim theories [5,6]. Furthermore, SAFT has shown great success in the simulation of polar fluids with non-ideal intermolecular interactions [7–10].

The interfacial effect between minerals and fluids is a non-ideal interaction and its significant role in thermodynamic modeling has been recognized [11]. On one hand, it is imperative to develop our understanding about fluid-mineral governing interactions for precise assessment of fluid recovery from geological media. On the other hand,

* Corresponding author at: Department of Geosciences, University of Oslo, P.O. Box 1047 Blindern, 0316 Oslo, Norway.
E-mail address: sajjadah@uio.no (S. Ahmadi Goltapeh).

https://doi.org/10.1016/j.seta.2021.101624
Received 25 May 2021; Received in revised form 3 August 2021; Accepted 14 September 2021
Available online 2 October 2021

Nomenclature

A	Helmholtz free energy [kcal]
a	Intensive Helmholtz free energy [kcal/mol]
E_{conf}	Configurational energy [kcal]
E_u/k	Dispersion energy parameter [K]
F_p	Local distribution of the molecules inside the interface region
F_{pr}	Fraction of the confined molecules in the square well of interface region
H	Hamiltonian [kcal/mol]
k	Boltzmann constant
K_E	Kinetic Energy [kcal/mol]
L	Length of the water bulk mounted above calcite [Å]
M_{int}	Internal partition function
m	Particle mass [kg]
m^{seg}	Segment number
N	Total number of particles
p	Momentum [kg.m/s]
P_E	Potential energy [kcal/mol]
Q	Partition function
r	Position [m]
T	Temperature[K]
V	Volume [$Å^3$]

Greek Letters

α	Number of adsorbed water molecules to the calcite surface
σ'	Segment diameter [Å]
σ	Average molecular diameter [Å]
λ	Broglie wavelength [Å]
ε	Attractive potential of molecule-wall interaction [kcal/mol]
$\varepsilon^{A_iB_i}$	Association energy parameter [K]
ρ	Density under confinement [kg/m^3]
$\kappa^{A_iB_i}$	Association volume
δ	Square well width [Å]
μ	Chemical potential [kcal/mol]

Subscripts and Superscripts

ass	Association
conf	Configurational
conf-ff	Configurational due to fluid–fluid interaction
conf-fw	Configurational due to fluid-wall interaction
diss	Dissociation
f	free
ff	Fluid-Fluid
fw	Fluid-Wall
hs	Hard sphere
i,j	counter
int	Internal
max	maximum
z	Z-axis

cubic EOSs are not suitable candidates to capture the molecular interactions of fluid-mineral. In this regard, SAFT-type EOSs with some modifications and tunings are probably able to capture the fluid-rock mutual interactions. However, an experimental data set illustrating fluid-rock interactions is required for such SAFT modifications.

Herein, Molecular Dynamic (MD) simulation is introduced to provide insights on confined fluid properties. This approach considers the simulation outcomes as pseudo experimental data to develop a new model [12]. The molecular simulation inspired by MD is able to simulate the fluid-mineral interface with known chemistry. MD simulations have emerged as a suitable technique to study the interfacial effects in systems containing complex fluids [13]. Recently, the study of fluid-rock interface with MD simulation has gained numerous contributions in the literature [14–16]. Kirch et al.[17] have studied the mutual effect of calcite interface and electrolyte ions (Na, Cl, and Ca) on water structure with MD modeling and Nuclear Magnetic Resonance (NMR). They illustrated that the strong ordering of surface water on calcite interface inhibits the adsorptions of chemical species. Ricci et al.[18] investigated the water-calcite interface with Atomic Force Microscopy (AFM) experiments and MD simulation. With MD simulation, they observed a shorter residence of Ca^{2+} ions than Na^{+} ions on the calcite surface, and they validated this finding with AFM experiment.

Few studies have looked at the impact of a mineral on the interface characteristics, and even fewer studied have utilized MD modeling to modify the EOS in which interface properties are computed. This research not only uses MD simulation to investigate the function of a particular mineral, such as calcite, on interface characteristics, but it also offers a method for calculating confinement parameters and incorporating them into Perturbation-Chain SAFT (PC-SAFT) [19] to measure interface properties.

In this study, we added calcite ($CaCO_3$) wall effect into the PC-SAFT, which led to the definition of confinement parameters. We modeled the water-calcite interface with MD technique to estimate the confinement parameters. Calcite (1014) surface was chosen to represent a carbonate rock (oil reservoir rock) because calcite is the most abundant and ubiquitous mineral in large carbonate reservoirs. Water, considered to be pure, is also one of the petroleum constituents with strong polar behavior. The estimated confinement parameters by MD were replaced in the modified PC-SAFT. Finally, PC-SAFT results were compared with the MD outcomes.

The remainder of this paper is organized as follows. In Section2, we describe the theoretical method for PC-SAFT modification and details of MD simulation. In Section 3, the modified PC-SAFT model is validated with MD results. In Section 4, we summarize the list of findings and conclusions.

Theoretical background

Modification on PC-SAFT equation of state

Figure 1 displays the scheme of the interfacial confinement between water and calcite. Three different regions are visible in this sketch. Region I displays the bulk region where water-water interactions govern the intermolecular interactions. Here, L_z is the distance from the water bulk top layer to the calcite surface. The thickness of L_z were 25 Å, 40 Å and 70 Å in MD simulations. Region II with thickness of δ is the surface-adsorbed zone where the water-calcite interactions are dominant interactions. Region III is free of any water molecule because its thickness ($\sigma_i/2$) is less than half of the water molecules diameter ($\sigma_i/2 \leq 0.5$ Å) [20]. In other words, the thickness of this region is very narrow such that no water molecule could reside there. Within the confined geometry presented in Fig. 1, homogeneous and heterogeneous phase interactions mainly control the fluid phase behavior. The interactions in homogeneous and heterogeneous phases apply to the water-water and water-calcite, respectively.

Equation (1) shows a square-well potential, which estimates the interaction between the water molecules, where r_{ij} is the distance between two molecules, ε_{ij} is the depth of the square well, δ_{ij} is the relevant width of square well, and σ_{ij} is defined as the mean molecular diameter for water.

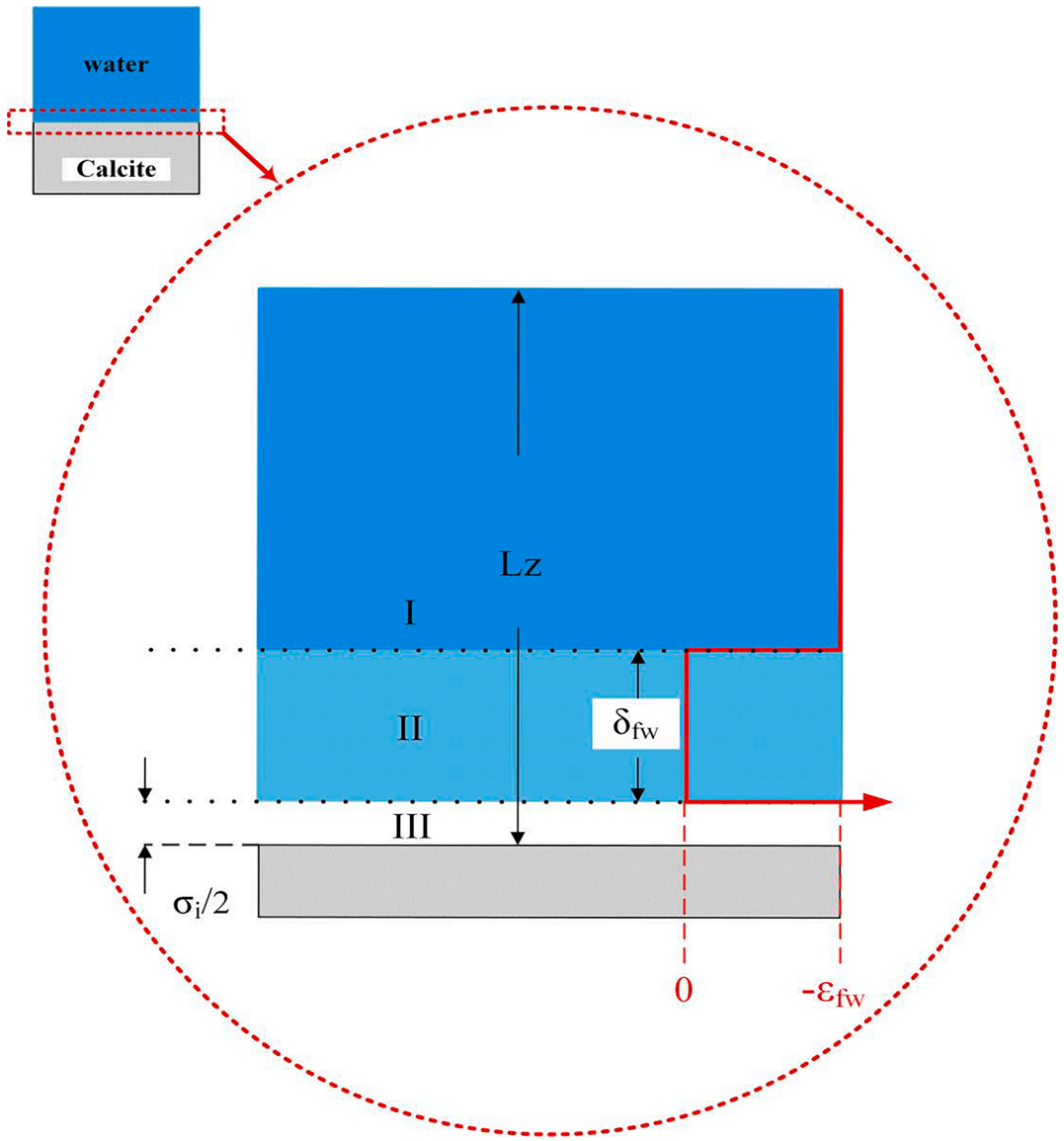

Fig. 1. Illustration of the confinement within water-calcite interface. Three different regions are visible here. Region I is the bulk region where molecular interactions are governed by water-water interactions. Lz is the distance from the water bulk top layer to the calcite surface, which is assumed to be 25 Å, 40 Å and 70 Å in MD simulations. Region II is the surface-adsorbed region where the molecular interactions are governed by water-calcite interactions and its thickness is shown by δ. Region III is forbidden zone, which is supposed to include no water molecule. This region, marking with σ, is very narrow such that the center of mass of water molecules cannot reside here.

$$u_{ij}(r_{ij}) = \begin{cases} \infty & r_{ij} < \sigma_{ij} \\ -\varepsilon_{ij} & \sigma_{ij} < r_{ij} < \sigma_{ij} + \delta_{ij} \\ 0 & r_{ij} > \sigma_{ij} + \delta_{ij} \end{cases} \quad (1)$$

Similarly, water and calcite molecules are supposed to interact through a square well, which is defined in equation (2):

$$u_i(l_i) = \begin{cases} \infty & l_i < \frac{\sigma_i}{2} \\ -\varepsilon_{fw,i} & \frac{\sigma_i}{2} < l_i < \frac{\sigma_i}{2} + \delta_{fw} \\ 0 & l_i > \frac{\sigma_i}{2} + \delta_{fw} \end{cases} \quad (2)$$

According to equation (2), $\varepsilon_{fw,i}$ moves toward infinite within region III. Therefore, the landing of the water molecules in this narrow region is not probable. Hereafter, $L_z/(0.5\sigma_i)$ is called length-ratio (L-R), showing the dimensionless water thickness in the water-calcite system.

In this context, we used Travalloni et. al.[21], approach to modify PC-SAFT EOS. To modify PC-SAFT equation of state, it is required to start from the original definition of partition function, because partition function provides a theoretical platform to derive the thermodynamic properties. General definition of partition function is given in equation (3) [22]:

$$Q(N,V,T) = \left(\frac{M_{int}^N}{\lambda^{3N}N!}\right) v_f^N exp\left(\int_\infty^T \frac{E_{conf}}{kT^2} dT\right) \quad (3)$$

On the left side of equation (3) are the total number of particles (N), the system volume (V), and the temperature (T). On the right side, M_{int} is the internal partition function, λ is the de Broglie thermal wavelength, E_{conf} is configurational energy and k is the Boltzmann constant. The general definitions of Helmholtz free energy and chemical potential are written as:

$$A(N,V,T) = -kT\ Q(N,V,T) \quad (4)$$

$$\mu = \left(\frac{\partial A}{\partial N}\right)_{T,V} \quad (5)$$

The term of Helmholtz energy for water-water interaction in the homogeneous phase (region I) can be defined with equations (1), (3), and (4). To complete the thermodynamics of the system, it is required to add the wall effect contribution into the partition function. Equation (6) includes the effect of the calcite wall on water-calcite interface. As can be observed, the configurational energy contribution has been split into fluid–fluid and fluid-wall:

$$Q(N,V,T) = \left(\frac{M_{int}^{N}}{\lambda^{3N}N!}\right) v_f^N \, exp\left(\int_{\infty}^{T} \frac{E_{conf-ff}}{kT^2} dT\right) exp\left(\int_{\infty}^{T} \frac{E_{conf-fw}}{kT^2} dT\right) \quad (6)$$

In equation (6), $E_{conf\text{-}ff}$ and $E_{conf\text{-}fw}$ denote contributions of fluid–fluid and fluid-wall interactions, respectively. The first three terms in the right hand side ofequation (6) correspond to the Helmholtz free energy in the bulk phase and the last term applies to the Helmholtz free energy within the interface confinement. In other words, equation (3) is modified to equation (6) by adding a fluid-wall contribution. Substitution of Helmholtz free energy in bulk phase gives:

$$\begin{aligned} Q(N,V,T) &= exp\left(-\frac{A^{ff}}{kT}\right) \times exp\left(\int_{\infty}^{T} \frac{E_{conf-fw}}{kT^2} dT\right) \\ &= exp\left(-\frac{A^{ff}}{kT}\right) \times exp\left(-\frac{A^{fw}}{kT}\right) \end{aligned} \quad (7)$$

A^{ff} in equation (7) shows the Helmholtz free energy in the bulk phase. Additionally, the integral product of the second component in the right hand side of equation (7) has been replaced with A^{fw}, which stands for Helmholtz free energy for water-calcite interaction.

The natural logarithm of equation (7) gives:

$$ln\ Q(N,V,T) = -\frac{1}{kT}\left(A^{ff} + A^{fw}\right) \quad (8)$$

In equation (9), the terms of Helmholtz free energy corresponds to the calcite wall effect has been presented separately:

$$\left(\frac{A^{fw}(N,V,T)}{kT}\right) = \left(-\int_{\infty}^{T} \frac{E_{conf-fw}}{kT^2} dT\right) \quad (9)$$

Now, the partition function for water-calcite interface can be defined as a list of different terms, which contribute to total Helmholtz energy.

$$ln\ Q(N,V,T) = -\frac{1}{kT}\left(A^{hs} + A^{disp} + A^{assoc} + A^{fw}\right) \quad (10)$$

According to PC-SAFT, the Helmholtz contribution for bulk (A^{ff}) can be broken down into hard-sphere (A^{hs}), dispersion (A^{disp}), and association (A^{assoc}). It is worth to note that, in this simulation, water is assumed completely pure, namely no cation and anion exit in water bulk. Table 1 shows the pure component parameters of water used in PC-SAFT EOS [23].

Where m^{seg} is the segment diameter, E_u/k is the dispersion energy parameter, $\varepsilon^{A_iB_i}$is the association energy parameter, $\kappa^{A_iB_i}$is the association volume and σ' is the segment diameter determined using the formula in Table 1.

To make an intensive term, N is added to the denominator, which gives:

$$ln\ Q(N,V,T) = \tilde{a}^{hs} + \tilde{a}^{dis} + \tilde{a}^{ass} + \tilde{a}^{fw} \quad (11)$$

Equation (11) expresses the partition function in terms of well-defined Helmholtz energy contributions. To estimate a^{fw}, we have applied equation (12) which uses F_p to relate the energy parameter of water-calcite to configurational energy [21]:

$$E_{conf-fw} = -NF_p\varepsilon_{fw} \quad (12)$$

In equation (12), ε_{fw} is the energy parameter associated with water-calcite interaction. F_p also is defined as:

$$F_p = F_{pr} + \left(1 - F_{pr}\right)\left(1 - exp\left(\frac{-\varepsilon_{fw}}{kT}\right)\right)\left(1 - \frac{\rho}{\rho_{max}}\right)^{\theta} \quad (13)$$

According to Travalloni et. al. [21], θ and F_{pr} are confinement degree and fraction of the water molecules in the square well. The equations (14) and (15) present θ and F_{pr} definitions, based on the depicted assumptions in Fig. 1:

$$F_{pr} = \frac{\left(L_Z - \frac{\sigma}{2}\right) - \left(L_Z - \frac{\sigma}{2} - \delta\right)}{\left(L_Z - \frac{\sigma}{2}\right)} \quad (14)$$

$$\theta = \frac{L_Z}{\delta + \frac{\sigma}{2}} \quad (15)$$

where L_z is length of water bulk mounted over calcite wall, δ is width of the square well, and σ is average dimeter of the water molecules.

In order to compute the Helmholtz free energy incorporating calcite-wall effect, ε_{fw}, ρ_{max}, θ and F_{pr} must be calculated in advance using MD simulation. In the next step, F_p is computed using confinement parameters mentioned before. Calculated F_p is put into equation (12) and the results are plugged into equation (9). The integral product of $E_{conf\text{-}fw}$ is then used to calculate A_{fw} in equation (9). Equation (10), which sums up the Helmholtz species, yields the Helmholtz free energy corresponds to the interface confinement.

MD simulation

The MD simulation applies the Born-Oppenheimer approximation to model the dynamics of the multi-particle systems built upon a certain thermodynamic ensemble [24]. In this approximation, Newton's law of motion governs the dynamic of the nuclei corresponding to the atoms or molecules. Therefore, the non-relativistic Hamiltonian becomes an implicit function of nuclei positions and momentums [25]:

$$H(p,r) = K_E + U = \sum_{i=1}^{N} \frac{p_i^2}{2m_i} + U(r_1 + r_2 + \ldots + r_i + \ldots + r_N) \quad (16)$$

Where p_i and r_i are set of particle momenta and positions, K_E is kinetic energy, U(r) is potential energy, m_i is particle mass, and N is the total number of particles.

We used the open source LAMMPS software as the classical molecular dynamic code for molecular dynamic simulation [26]. The Newtonian equation of motions developed by the velocity Verlet algorithm adopts the time step of 1 fs for all simulations. Each MD simulation was executed with a constant temperature. The temperature itself was updated through a loop in the LAMMPS code.

The developed force field by Zhao et al. [27] defined the internal forces between 480 calcite molecules. These molecules are sorted into 6 layers along (1014) a perfect calcite surface. The SPC/E [28,29] model described the internal interactions among the molecules of water bulk. Fig. 2 shows the calcite-water layout in the simulation box. As it is seen, we have built a molecular system including a water bulk mounted above the calcite slab along the z-direction. In the simulation box, water bulk was prepared with three different lengths along the z-axis: 25 Å, 40 Å, and 70 Å. For both the x and y directions, the boundary conditions were periodic. The boundary condition for the z-direction was set to be constant, and a reflecting wall was inserted above the water bulk to avoid atom loss.

To wrap the molecules of the calcite slab and water bulk, we applied

Table 1
PC-SAFT parameters for pure water.

m^{seg}	σ' [Å]	E_u/k [K]	$\varepsilon^{A_iB_i}$ [K]	$\kappa^{A_iB_i}$
1.2047	*	353.95	2425.7	0.0451

*$\sigma = 2.7927 + 10.11exp(-0.01775 \times T) - 1.417exp(0.01146 \times T)$, T is the temperature in [K]

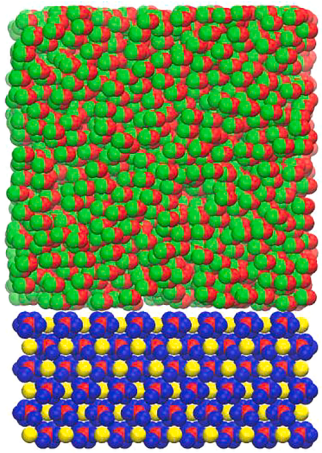

Fig. 2. Illustration of water-calcite system for MD simulation. The calcite slab includes 6 layers sorted along the (1014) plane and overlaps with water bulk on xy plane. The water bulk has extended along the z-axis with 25 Å, 40 Å and 70 Å thickness.

PACKMOL [30] that compacts the molecules with a certain distance such that the structure of molecules remains intact. Running the minimize function with conjugate gradient algorithm lets the molecules remain at a reasonable distance and the energy flood during the simulation run is avoided. The equilibration process in each simulation is fulfilled by initializing the particles velocity with a set temperature. Then, the equilibration followed by Nose-Hoover NVT thermostat until 3 ns in which temperature remains constant at T = 300 K, 400 K and 500 K. Finally, LAMMPS measured the thermodynamic properties by averaging over total run time.

Results and discussion

Density profile at constant length ratio

Figure 3 illustrates the profile of water density inside the layering zone and bulk phase. The length-ratio (L-R) and temperature, respectively in each row and column, are constant. From left to right the simulation temperature increases from 300 K to 400 K and 500 K while from top to bottom the L-R decreases from 140 to 80 and 50. The density plot has oscillatory behavior near the calcite-wall so-called layering zone. In fact, the layering zone and bulk imply regions II and I according to the zone classification in Fig. 1.

In the first row with L-R = 140, when T = 300 K, the density experience the longest peak in region II and flatten at bulk density inside region I. However, the shortest peak in region II and minimum density inside region I belongs to T = 500 K. Simultaneously, the density values at T = 400 K remain between T = 300 K and T = 500 K. Compared with the first row, the same regime is observed in the second and third row for L-R = 80 and L-R = 50, respectively. It means, with constant L-R, the highest density inside region I and II belongs to T = 300 K. Whilst the lowest density in region I and II corresponds to T = 500 K. Therefore, for a constant L-R, the density inside the region I and region II varies with respect to the mean distance between the water molecules. In other words, with constant length-ratio, T = 300 K, 400 K and 500 K provide the minimum, medium and maximum mean distance among the water molecules, which respectively leads to maximum, medium and minimum density in region I and II.

Density profile at a constant temperature

The first, second and third column in Fig. 3 display density profile at constant temperature and different L-R values. A deceptive point that one may notice at first glance is the ascending behavior of the density profile from top to bottom. Namely, the longest and shortest peak in region II occur at L-R = 50 and L-R = 140. Within region I from top to bottom, on the other hand, the density trend of L-R = 140, lays on higher values than L-R = 80 and L-R = 50. In Fig. 3, this regime is repeated in all columns.

For ease of comparison at constant temperature and variable L-R, the depicted density profiles in Fig. 3, have been normalized between 0 and 1. Fig. 4a–c display the variation of normalized density with respect to the L-R at constant temperature. In Fig. 4a–c, one can visually compare the size of the marked area showing average density. For example, at T = 300 K the smallest area belongs to L-R = 50 compared with L-R = 80 and L-R = 140. It means, L-R = 140 and L-R = 50 make the max and min average density at T = 300 K while the relevant density for L-R = 80 remains larger than L-R = 50 and smaller than L-R = 140. This regime is replicated in Fig. 4b and c. Therefore, with fixed temperature, the min and max length-ratio provide minimum and maximum average density within region II and I, respectively.

This fact is consistent with the definition of interface confinement within the water bulk and calcite-wall. To be specific, reduction in confinement size reduces the density, and raising the confinement size provides density growth. In our simulation, L-R = 140 is the maximum confinement and gives larger water density than L-R = 80 and L-R = 50. The maximum density is potentially achieved in a water-calcite system with an infinite length-ratio (L-R=∞) or a water bulk without the presence calcite-wall. Even though L-R = 140 and L-R = 50 give the greatest and lowest average density within regions II and I, how the local peaks inside region II are interpreted remains a mystery.

In fact, the adsorbed water molecules on the calcite-wall are apparent in the local peaks of region II. On the one hand, the number of water molecules adsorbed to the calcite surface is controlled by the calcite's attraction. On the other hand, the average attraction force inside region II, is the consequence of a trade-off between the calcite-wall attraction and the water bulk attraction. It means that thin layers of water are more attracted to the calcite-wall than thicker ones. Additionally, it may be said that $\alpha_{50} > \alpha_{80} > \alpha_{140}$ where α represents the number of water molecules within the first adsorbed layer, and the subscripts express the L-R values. Consequently, the extension of the water bulk along the z-axis increases the waterside's average attraction force and decreases water adsorption on the calcite-wall, and reducing the water length, on the other hand, results in a notable local peak of density inside region II. To sum up, the highest local density is achieved at the first adsorbed layer when the lowest confinement is used. However, as seen in Fig. 4a–c, the average density under minimum confinement remains minimal.

Energy behavior with respect to L-R and temperature variation

Figure 5 demonstrates the total energy profile inside region II and I for different length-ratios and temperatures. The vertical columns display the energy behavior at fixed temperature and L-R = 140, 80 and 50. The horizontal rows express the energy variation at constant L-R and T = 300 K, 400 K and 500 K. Moving from left to right where L-R = 140, one observe the decay in the absolute energy values such that $E_{300K} > E_{400K} > E_{500K}$. The same pattern is noticed in the second and third row, which means at constant length-ratio, higher temperature causes lower energy inside the layering zone and bulk.

From left to right, comparison of the energy profiles with the density trends in Fig. 3, reveals that max and min density within region II and I corresponds to the maximum and minimum energy respectively. For example, in the first row of Fig. 3 one notices $\rho_{300K} > \rho_{400K} > \rho_{500K}$. It means with T = 300 K the water molecules stand at shorter distance than T = 400 K and T = 500 K. Therefore, with constant L-R, the higher the temperature the lower the total energy.

Moving from top to bottom, one observes the length of local peaks within region II increases, whereas the widths of the curves narrow

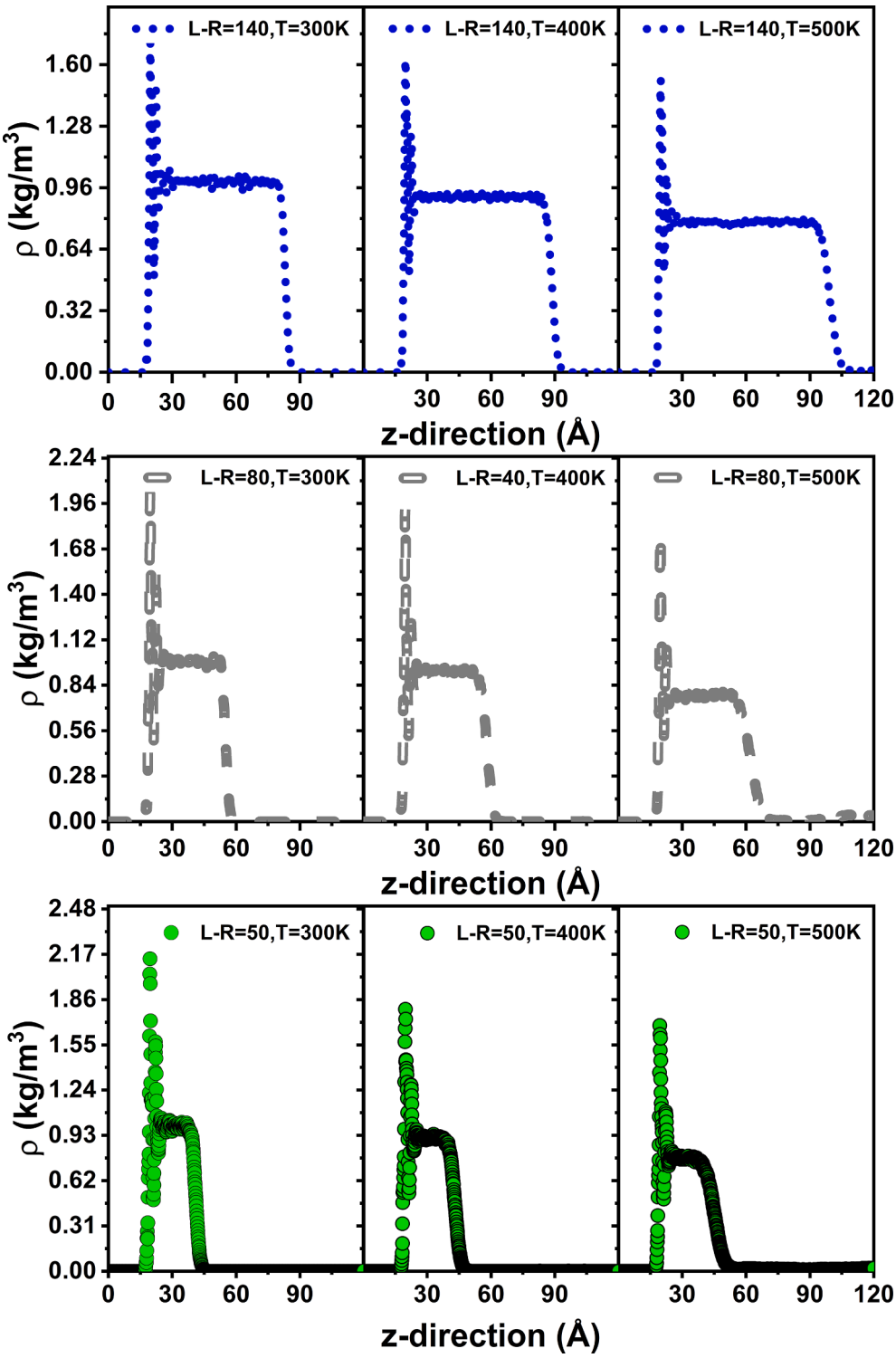

Fig. 3. Illustration of the density profile inside region I and II at several length-ratios and different temperatures. The plotted curves in each row represent the density profile at constant L-R, while each column presents the density profile at fixed temperature. From left to right the simulation temperature increases from 300 K to 400 K and 500 K. The L-R, from top to bottom, decreases from 140 to 80 and 40.

down. This energy pattern provides smaller average energy for smaller confinement and vice versa. For example, in the last column of Fig. 5 where T = 500 K, the absolute value of the integral over L-R = 50 trend corresponds to the minimum average energy. Whereas the absolute value of integral over L-R = 140 illustrates the maximum average energy. Therefore, with T = 500 K, the reduction in length-ratio reduces the absolute average total energy, i.e., $E_{140} > E_{80} > E_{50}$. This pattern is observed in the first and second columns.

To sum up, the stronger effect of the calcite attraction forces on thin bulk of water leads to the higher adsorption at the first adsorbed layer of water molecules over calcite-wall. High adsorption at the first adsorbed layer results short intermolecular distance. When the intermolecular distance at the first adsorbed layer diminishes, the length of the local peaks for density and energy increases. Whilst, thick bulk of water have

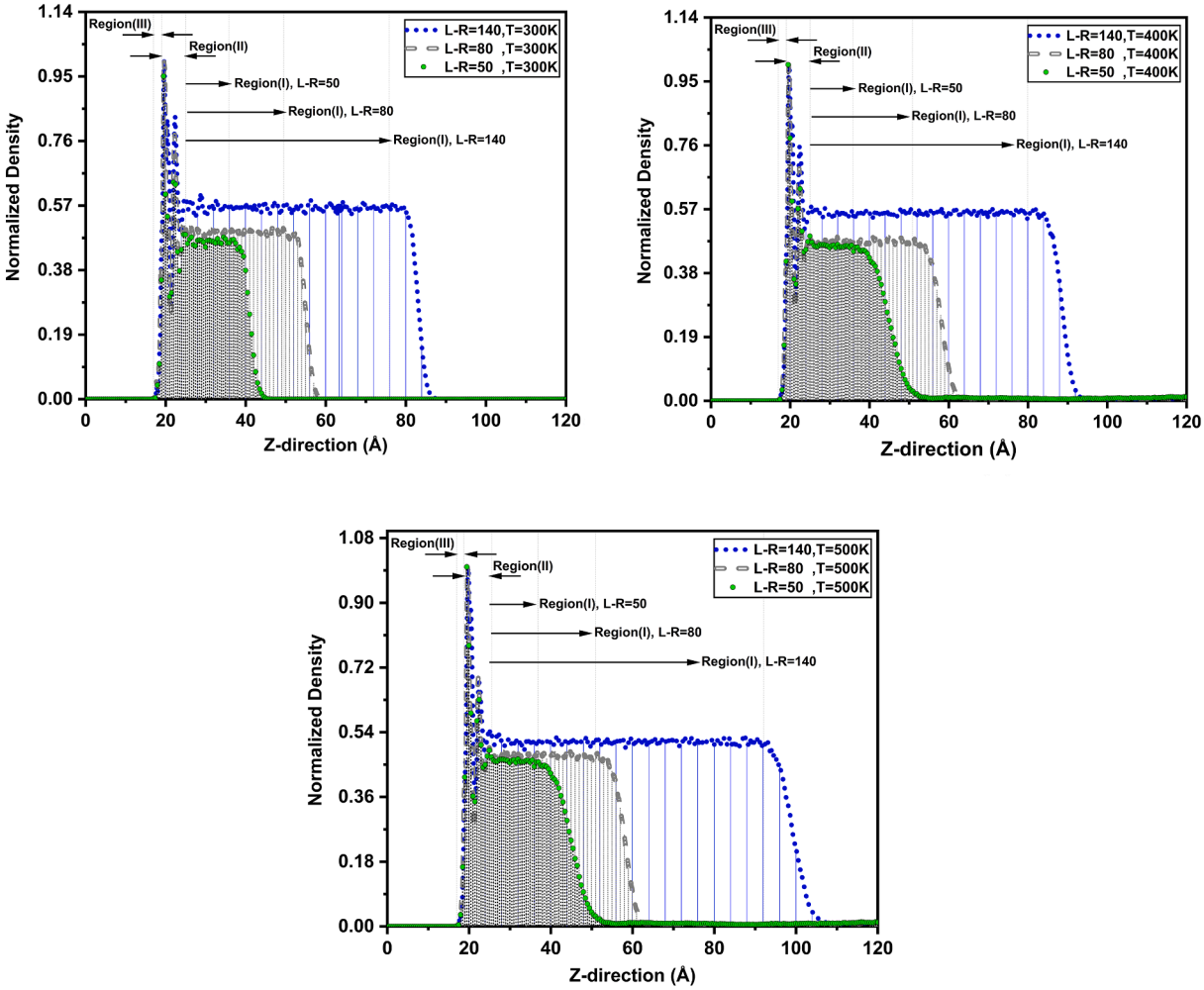

Fig. 4. Illustration of the density profile within region I and II at different L-R and constant temperature. The density is normalized between 0 and 1, which allows comparing the average density trend. The integral of the density inside region I and II is shown by the darkened regions beneath the trends (blue > gray > green). The greatest and lowest average densities at constant temperature, according to the shaded area under the curve, are L-R = 140 and L-R = 50, respectively. In addition, the marked up regions depict the skematic thickness of regions I, II, and III. (For interpretation of the references to colour in this figure legend, the reader is referred to the web version of this article.)

stronger intermolecular attractions and cancels out the effect of the calcite attraction. Hence, the density within the first adsorbed layer over the calcite-wall decreases. The reduction in density within the first adsorbed layer shortens the length of the local peaks for density and energy. Therefore, the shorter the water bulk the larger the local peak in density, but the smaller the average density. In addition, high and low values of average density correspond to the high and low values of average total energy, respectively. Therefore, with fixed L-R and variable temperature, the molecule–molecule distance controls the density and energy. Nevertheless, with variable L-R and fixed temperature, the balance between molecular attraction forces of calcite-wall and water bulk controls the density and energy.

Comparison of PC-SAFT and MD simulation

In section 2.1, the confinement parameters were introduced by equations (13), (14) and (15). We applied MD simulations to estimate the introduced confinement parameters. Table 2 presents calculated confinement parameters under different confinement sizes and temperatures. In this table, the potential of the water-calcite interaction (ε_{fw}) was calculated by the integral of the energy over the layering zone [31]. The fraction of confined molecules (F_{pr}) and confinement degree (θ) were determined according to the defined formula in equations (14) and (15).

To estimate the bulk density (ρ_{max}), we simulated water in MD without the presence of the calcite-wall. Because, at a known temperature, the density of water without the presence of the calcite-wall is maximum. Hence, water was simulated with MD at T = 300 K, 350 K, 400 K, 450 K, and 500 K which the results were tabulated in Table 3.

Table 3 displays simulation (MD and PC-SAFT) and laboratory results for water density without the presence of calcite-wall. To be specific, Table 3 reports the reliability of MD and PC-SAFT for predicting the water density without the presence of calcite-wall. The columns |RE-1| and |RE-2| show the absolute relative errors for MD and PC-SAFT, respectively. As shown, for a specific range of temperature, the obtained results from MD and PC-SAFT are reliable, although the absolute relative error increases with temperature rise.

Table 4 listed the predictions of MD and modified PC-SAFT for the interface layer within region II. One can compare Table 4 with Table 3 at relevant temperatures. As seen, because of the calcite-wall presence, the reported densities in Table 4 are smaller than the relevant ones in Table 3.

The plot in Fig. 6 compares the modified PC-SAFT with MD results at different temperatures. The diamond, circle and square exhibit the MD results at L-R = 50, 80 and 140, respectively. In addition, blue, red and green curves are representative of modified PC-SAFT predictions L-R =

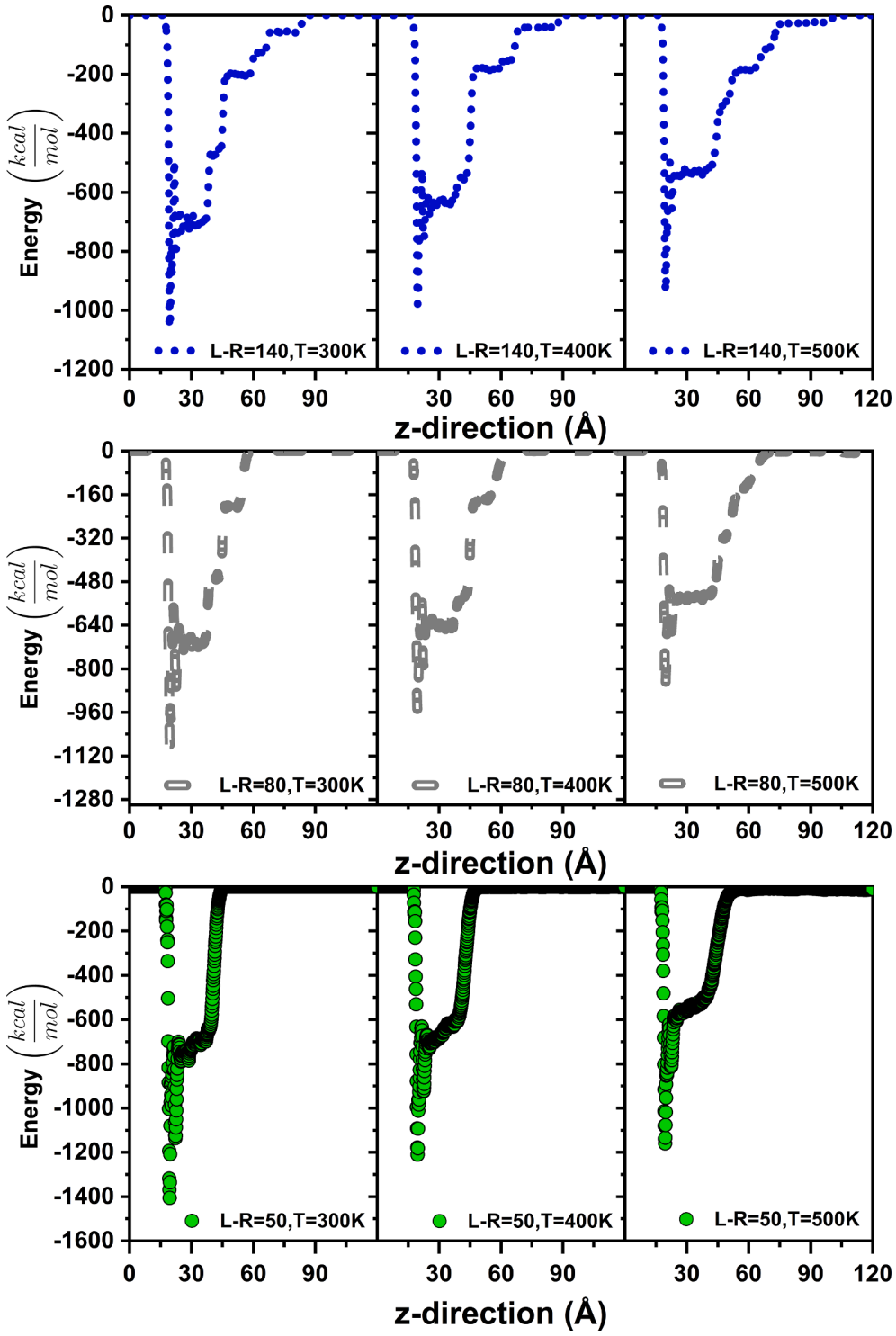

Fig. 5. Illustration of the energy profile inside region I and II at several length-ratios and different temperatures. The plotted figures in each row and column represent the energy trend at constant length-ratio (L-R) and temperature respectively. From left to right the simulation temperature increases from 300 K to 400 K and 500 K while from top to bottom the L-R decreases from 140 to 80 and 50.

50, 80, and 140. At the bottom of the plot box, the profile of absolute relative error shows the deviation of modified PC-SAFT from MD results. To be specific, dashed, dotted and doubled lines are the trajectory of relative error at L-R = 50, 80 and 140, respectively. The vertical axis at the left is the density ratio, including the bulk density in the denominator, which implies ρ_{max}.

As seen in Fig. 6, when L-R increases at a fixed temperature, both MD and PC-SAFT predict larger fractions of ρ/ρ_{max} [33]. This means with a fixed temperature, by growth in confinement size, the confined density (ρ) increases which leads to a reduction of the gap between ρ and ρ_{max}. This fact also satisfies the mathematical limit in equation (13), which says, by extending the water length above the calcite-wall ($L_z \rightarrow \infty$), the density within the layering zone approaches the bulk density ($\rho = \rho_{max}$). Substitution of $\rho = \rho_{max}$ in equation (13) gives homogeneous distribution within the region II ($F_p = F_{pr}$).

In addition, when the temperature rises for a fixed L-R, the MD

Table 2
Estimated confinement parameters with MD simulations. The ε_{fw}, ρ_{max}, F_{pr} and θ respectively present potential of fluid-wall interaction, bulk density, fraction of confined molecules and confinement degree.

T = 300 [K]					
L-R	ε_{fw} [kcal]	ρ_{max} [kg/m^3]	δ [Å]	F_{pr}	θ
50	−3248.525	957.650	5.6	0.229	3
80	−2686.685	973.203	5.9	0.149	6
140	−2695.768	982.393	6.1	0.087	10
T = 400 [K]					
50	−3023.907	888.010	5.6	0.229	3
80	−2511.321	898.869	5.9	0.149	6
140	−2497.062	905.682	6.1	0.087	10
T = 500 [K]					
50	−2722.839	770.170	5.6	0.229	3
80	−2246.411	774.076	5.9	0.149	6
140	−2271.883	780.998	6.1	0.087	10

Table 3
List of the water density at different temperatures without the presence of calcite-wall. This table compares the laboratory data with the outcomes of MD and PC-SAFT. The columns |RE-1| and |RE-2| display the absolute relative error for MD and PC-SAFT, respectively.

Liquid water density					
T [K]	Laboratory [32] [kg/m^3]	MD [kg/m^3]	PC-SAFT [kg/m^3]	|RE-1| %	|RE-2| %
300	996.499	1000.003	990.490	0.352	0.603
350	973.693	970.383	973.365	0.339	0.033
400	937.465	923.463	952.634	1.494	1.618
450	890.319	861.221	926.686	3.268	4.085
500	831.302	791.007	893.784	4.847	7.516

Table 4
Comparison between MD outcomes as a pseudo experiment and modified PC-SAFT for region II. As it is seen, when the temperature is fixed, PC-SAFT prediction grows with growth in L-R. While with constant L-R, PC-SAFT prediction decreases with temperature growth.

Region (II): Liquid water density						
T K	MD [kg/m^3]			Modified PC-SAFT [kg/m^3]		
	L-R = 50	L-R = 80	L-R = 140	L-R = 50	L-R = 80	L-R = 140
300	890.251	899.404	916.439	990.569	990.586	990.621
400	836.394	846.519	857.083	952.708	952.725	952.750
500	766.145	771.005	784.565	893.907	893.908	893.930

predicts a smaller ratio of $\rho/\rho_{max,}$ and relevant |RE| has increased. In other words, under a fixed confinement size, going up in temperature increases the gap between confined density and ρ_{max}. The behavior of the absolute relative error in Table 3 is consistent with the profile of |RE| in Fig. 6. Regarding the |RE| profile at the bottom, two factors result in smaller errors, i.e., the larger confinement and lower temperature. The former moves the properties of the confined water toward the properties of the water bulk, as discussed already. The latter refers to the accuracy of chosen model for water in MD simulation because the accuracy of SPC/E model deteriorates at high temperatures [34]. According to the hypothesis of SPC/E model, the water molecule is fixed-charge, rigid, and non-polarized with an on-plane location. However, in reality, the "charge–distances–angle" parameters for the water molecules fluctuate routinely, affecting the molecule's electrostatic, and therefore the consequence bulk properties. Because of high temperature, the limitations of SPC/E model to predict the water properties increases because i) at increasing temperatures, the spatial fluctuation of

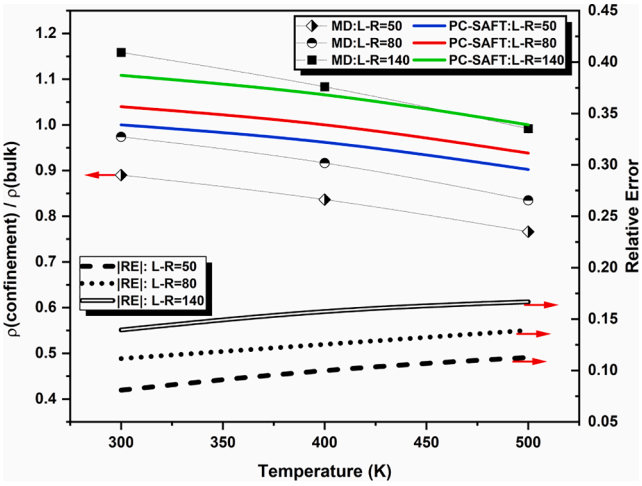

Fig. 6. Graph compares the predictions of MD and modified PC-SAFT at T = 300 K, 400 K and 500 K. The diamond, circle and square exhibit the MD results at L-R = 50, 80 and 140. The blue, red and green curves are representative of modified PC-SAFT predictions at L-R = 50, 80 and 140. In the bottom of plot box, the profile of absolute relative error shows the deviation of modified PC-SAFT from MD results. (For interpretation of the references to colour in this figure legend, the reader is referred to the web version of this article.)

"charge–distances–angle" rises. Therefore, the legitimacy of "simple 3-point charge" models diminishes ii) as temperature rises, the non-polarized assumption loses its validity due to increasing collision between the molecules. As a result, SPCE's ability to forecast water characteristics at high temperatures has deteriorated [35].

Summary and conclusions

To develop our understanding for confinement within fluid-rock interface we simulated water-calcite system with three different thickness of water bulk: L-R = 140, 80 and 50. In our numerical experiments, we observed that going down in water thickness at a fixed temperature, provides smaller density and energy within the water-calcite interface. Furthermore, with a constant L-R, low temperature give rise in density and energy within the layering zone. Then, we concluded that at constant L-R mean distance between water molecules controls the density and energy trend. Whereas at constant temperature the attraction forces of calcite control the density and energy profile. To develop a thermodynamic model for predicting the density change due to calcite-wall presence, we defined a new contribution for Helmholtz free energy in PC-SAFT. Then, the introduced confinement parameters: potential of fluid-wall interaction (ε_{fw}), bulk density (ρ_{max}), fraction of confined molecules (F_{pr}) and confinement degree (θ) were adjusted against MD calculations. The prediction of modified PC-SAFT were validated with MD and good agreement was observed. The uncertainty of the modified PC-SAFT increases with reduction in confinement or temperature.

In conclusion, MD simulation demonstrates that at the water-calcite interface, a smaller L-R provides a lower density at given temperature while low temperatures increase density and energy with a given L-R. Furthermore, the density, energy, and geometry of confinement at the layering zone influence the derived contribution for Helmholtz free energy. Finally, as a result of the addition of introduced Helmholtz energy to PC-SAFT, one may anticipate the interface properties in good agreement with MD results.

CRediT authorship contribution statement

S. Ahmadi G.: Conceptualization, Methodology, Software, Validation, Writing – original draft, Visualization, Formal analysis, Investigation, Writing - review & editing. **S. Abdolahi:** Software, Validation,

Investigation. **R. Miri:** Supervision, Writing - review & editing. **H. Hellevang:** Supervision, Writing - review & editing.

Declaration of Competing Interest

The authors declare that they have no known competing financial interests or personal relationships that could have appeared to influence the work reported in this paper.

References

[1] Qiu X, Yang H, Dejam M, Tan SP, Adidharma H. Experiments on the capillary condensation/evaporation hysteresis of pure fluids and binary mixtures in cylindrical nanopores. J Phys Chem C 2021;125:5802–15.
[2] Nikpoor MH, Dejam M, Chen Z, Clarke M. Chemical–gravity–thermal diffusion equilibrium in two-phase non-isothermal petroleum reservoirs. Energy Fuels 2016; 30:2021–34.
[3] Sengers JV, Kayser RF, Peters CJ, White HJ. Equations of state for fluids and fluid mixtures. Elsevier; 2000.
[4] Rowlinson JS. JD van der Waals: On the Continuity of the Gaseous and Liquid States. North-Holland; 1988.
[5] Barker JA, Henderson D. Perturbation theory and equation of state for fluids. II. A successful theory of liquids. J Chem Phys 1967;47:4714–21.
[6] Wertheim MS. Fluids with highly directional attractive forces. IV. Equilibrium polymerization. J Stat Phys 1986;42:477–92.
[7] Chapman WG, Jackson G, Gubbins KE. Phase equilibria of associating fluids: chain molecules with multiple bonding sites. Mol Phys 1988;65:1057–79.
[8] Chapman WG, Gubbins KE, Jackson G, Radosz M. New reference equation of state for associating liquids. Ind Eng Chem Res 1990;29:1709–21.
[9] Tan SP, Adidharma H, Radosz M. Recent advances and applications of statistical associating fluid theory. Ind Eng Chem Res 2008;47:8063–82.
[10] Michelsen ML, Mollerup J. Thermodynamic modelling: fundamentals and computational aspects. Tie-Line Publications 2004.
[11] Sedghi M, Piri M, Goual L. Atomistic molecular dynamics simulations of crude oil/ brine displacement in calcite mesopores. Langmuir 2016;32:3375–84.
[12] Cárdenas H, Müller EA. Extension of the SAFT-VR-Mie equation of state for adsorption. J Mol Liq 2019;294:111639.
[13] Ghatee MH, Koleini MM, Ayatollahi S. Molecular dynamics simulation investigation of hexanoic acid adsorption onto calcite (101 4) surface. Fluid Phase Equilib 2015;387:24–31.
[14] Bourg IC, Lee SS, Fenter P, Tournassat C. Stern layer structure and energetics at mica–water interfaces. J Phys Chem C 2017;121:9402–12.
[15] Yousefi F, Khoeini F, Rajabpour A. Thermal rectification and interfacial thermal resistance in hybrid pillared-graphene and graphene: a molecular dynamics and continuum approach. Nanotechnology 2020;31:285707.
[16] Adapa S, Swamy DR, Kancharla S, Pradhan S, Malani A. Role of mono-and divalent surface cations on the structure and adsorption behavior of water on mica surface. Langmuir 2018;34:14472–88.
[17] Kirch A, Mutisya SM, Sánchez VM, de Almeida JM, Miranda CR. Fresh molecular look at calcite–brine nanoconfined interfaces. J Phys Chem C 2018;122:6117–27.
[18] Ricci M, Spijker P, Stellacci F, Molinari J-F, Voïtchovsky K. Direct visualization of single ions in the Stern layer of calcite. Langmuir 2013;29:2207–16.
[19] Gross J, Sadowski G. Perturbed-chain SAFT: an equation of state based on a perturbation theory for chain molecules. Ind Eng Chem Res 2001;40:1244–60.
[20] D'Arrigo JS. Screening of membrane surface charges by divalent cations: an atomic representation. Am J Physiol Physiol 1978;235:C109–17.
[21] Travalloni L, Castier M, Tavares FW, Sandler SI. Thermodynamic modeling of confined fluids using an extension of the generalized van der Waals theory. Chem Eng Sci 2010;65:3088–99.
[22] Hill TL. An introduction to statistical thermodynamics. Courier Corporation 1986.
[23] Fuchs D, Fischer J, Tumakaka F, Sadowski G. Solubility of amino acids: Influence of the pH value and the addition of alcoholic cosolvents on aqueous solubility. Ind Eng Chem Res 2006;45:6578–84.
[24] Born M, Oppenheimer R. Ann. Phys. 1927.
[25] Landau LD. EM Lifshitz Statistical Physics. Course Theor Phys 1980;5:396–400.
[26] Plimpton S. Fast parallel algorithms for short-range molecular dynamics. J Comput Phys 1995;117:1–19.
[27] Zhao J, Yao G, Ramisetti SB, Hammond RB, Wen D. Molecular dynamics investigation of substrate wettability alteration and oil transport in a calcite nanopore. Fuel 2019;239:1149–61.
[28] Berendsen HJC, Grigera JR, Straatsma TP. The missing term in effective pair potentials. J Phys Chem 1987;91:6269–71.
[29] Vega C, Abascal JLF. Simulating water with rigid non-polarizable models: a general perspective. Phys Chem Chem Phys 2011;13:19663–88.
[30] Martínez L, Andrade R, Birgin EG, Martínez JM. PACKMOL: a package for building initial configurations for molecular dynamics simulations. J Comput Chem 2009; 30:2157–64.
[31] Tarazona P, Evans R. A simple density functional theory for inhomogeneous liquids: Wetting by gas at a solid-liquid interface. Mol Phys 1984;52:847–57.
[32] Doble M. Perry's chemical engineers' handbook. New York, USA: McGraw-Hill; 2007.
[33] Knight AW, Kalugin NG, Coker E, Ilgen AG. Water properties under nano-scale confinement. Sci Rep 2019;9:1–12.
[34] Shi B, Sinha S, Dhir VK. Molecular dynamics simulation of the density and surface tension of water by particle-particle particle-mesh method. J Chem Phys 2006;124: 204715.
[35] Izadi S, Onufriev AV. Accuracy limit of rigid 3-point water models. J Chem Phys 2016;145:74501.